

Thermodynamic criterion for searching high mobility two-dimensional electron gas at $KTaO_3$ interface

Wen-Xiao Shi(时文潇), Hui Zhang(张慧), Shao-Jin Qi(齐少锦), Jin-E Zhang(张金娥), Hai-Lin Huang(黄海林), Bao-Gen Shen(沈保根), Yuan-Sha Chen(陈沅沙), and Ji-Rong Sun(孙继荣)

Citation: Chin. Phys. B, 2021, 30 (**7**): 077302. DOI: 10.1088/1674-1056/ac078c
Journal homepage: http://cpb.iphy.ac.cn; http://iopscience.iop.org/cpb

What follows is a list of articles you may be interested in

Ferroelectric effect and equivalent polarization charge model of $PbZr_{0.2}Ti_{0.8}O_3$ on AlGaN/GaN MIS-HEMT

Yao-Peng Zhao(赵垚澎), Chong Wang(王冲), Xue-Feng Zheng(郑雪峰), Xiao-Hua Ma(马晓华), Ang Li(李昂), Kai Liu(刘凯), Yun-Long He(何云龙), Xiao-Li Lu(陆小力) and Yue Hao(郝跃)
Chin. Phys. B, 2021, 30 (**5**): 057302. DOI: 10.1088/1674-1056/abd469

Analysis of the decrease of two-dimensional electron gas concentration in GaN-based HEMT caused by proton irradiation

Jin-Jin Tang(汤金金), Gui-Peng Liu(刘贵鹏), Jia-Yu Song(宋家毓), Gui-Juan Zhao(赵桂娟), and Jian-Hong Yang(杨建红)
Chin. Phys. B, 2021, 30 (**2**): 027303. DOI: 10.1088/1674-1056/abbbf7

Electric gating of the multichannel conduction in $LaAlO_3/SrTiO_3$ superlattices

Shao-Jin Qi(齐少锦), Xuan Sun(孙璇), Xi Yan(严曦), Hui Zhang(张慧), Hong-Rui Zhang(张洪瑞), Jin-E Zhang(张金娥), Hai-Lin Huang(黄海林), Fu-Rong Han(韩福荣), Jing-Hua Song(宋京华), Bao-Gen Shen(沈保根), and Yuan-Sha Chen(陈沅沙)
Chin. Phys. B, 2021, 30 (**1**): 017301. DOI: 10.1088/1674-1056/abc54c

Enhanced spin-dependent thermopower in a double-quantum-dot sandwiched between two-dimensional electron gases

Feng Chi(迟锋), Zhen-Guo Fu(付振国), Liming Liu(刘黎明), Ping Zhang(张平)
Chin. Phys. B, 2019, 28 (**10**): 107305. DOI: 10.1088/1674-1056/ab3f98

Short-gate AlGaN/GaN high-electron mobility transistors with BGaN buffer

Tie-Cheng Han(韩铁成), Hong-Dong Zhao(赵红东), Xiao-Can Peng(彭晓灿)
Chin. Phys. B, 2019, 28 (**4**): 047302. DOI: 10.1088/1674-1056/28/4/047302

RAPID COMMUNICATION

Thermodynamic criterion for searching high mobility two-dimensional electron gas at $KTaO_3$ interface*

Wen-Xiao Shi(时文潇)[1,2], Hui Zhang(张慧)[1,2], Shao-Jin Qi(齐少锦)[1,2], Jin-E Zhang(张金娥)[1,2], Hai-Lin Huang(黄海林)[1,2], Bao-Gen Shen(沈保根)[1], Yuan-Sha Chen(陈沅沙)[1,3,†], and Ji-Rong Sun(孙继荣)[1,4,5,‡]

[1] *Beijing National Laboratory for Condensed Matter Physics and Institute of Physics, Chinese Academy of Sciences, Beijing* 100190, *China*
[2] *School of Physical Sciences, University of Chinese Academy of Sciences, Beijing* 100049, *China*
[3] *Fujian Innovation Academy, Chinese Academy of Sciences, Fuzhou* 350108, *China*
[4] *Songshan Lake Materials Laboratory, Dongguan* 523808, *China*
[5] *Spintronics Institute, University of Jinan, Jinan* 250022, *China*

(Received 1 February 2021; revised manuscript received 22 March 2021; accepted manuscript online 3 June 2021)

Two-dimensional electron gases (2DEGs) formed at the interface between two oxide insulators present a promising platform for the exploration of emergent phenomena. While most of the previous works focused on $SrTiO_3$-based 2DEGs, here we took the amorphous-ABO_3/$KTaO_3$ system as the research object to study the relationship between the interface conductivity and the redox property of B-site metal in the amorphous film. The criterion of oxide–oxide interface redox reactions for the B-site metals, Zr, Al, Ti, Ta, and Nb in conductive interfaces was revealed: the formation heat of metal oxide, ΔH_f^o, is lower than −350 kJ/(mol O) and the work function of the metal Φ is in the range of 3.75 eV$< \Phi <$ 4.4 eV. Furthermore, we found that the smaller absolute value of ΔH_f^o and the larger value of Φ of the B-site metal would result in higher mobility of the two-dimensional electron gas that formed at the corresponding amorphous-ABO_3/$KTaO_3$ interface. This finding paves the way for the design of high-mobility all-oxide electronic devices.

Keywords: two-dimensional electron gas, oxygen vacancies, thermodynamic criterion, Hall mobility

PACS: 73.20.–r, 68.35.Md, 73.40.–c **DOI:** 10.1088/1674-1056/ac078c

1. Introduction

In 2004, Ohtomo and Hwang discovered a metallic conductive interface between insulating oxides $SrTiO_3$ (STO) and $LaAlO_3$,[1] opening a new avenue for oxide electronics research. Since then, researchers have carried out a lot of works on the oxide heterojunctions based on STO substrates,[2–12] and a series of novel physical properties are revealed, such as two-dimensional superconductivity,[13,14] interfacial magnetism,[15–17] quantum Hall effect,[18] and efficient spin-to-charge conversion.[19,20] With the deepening of research, Zou *et al.*[21] discovered a new two-dimensional electron gas (2DEG) at the interface of $LaTiO_3$/$KTaO_3$ (KTO) system. KTO is similar to STO in many aspects. It exhibits a high dielectric constant[22] and is quantum paraelectricity.[23] However, it is different from STO by owning a strong atomic spin–orbit coupling,[24] about 20 times as high as that of STO. Therefore, distinct features are expected for the corresponding 2DEG. Comparing with the investigations on STO-based 2DEG, the work on KTO-based 2DEG is limited. In addition to the work of Zou *et al.*, the only reported 2DEGs at bilayer interfaces are amorphous-$LaAlO_3$/KTO[25,26] and EuO/KTO.[27] Effects associated with the distinct characters of KTO are far from being fully explored.

Herein, we take the amorphous-ABO_3/KTO system as the research object to study the relationship between the interface conductivity and the redox property of B-site metal in the amorphous film. Firstly, we report on the fabrication of a series of high-quality amorphous-ABO_3/KTO heterostructures. Secondly, the electric properties, such as the dependence of the sheet resistance (R_s) on temperature (T) and Hall resistance (R_{xy}), were measured. Finally, we adopted the formation heat of metal oxide, ΔH_f^o, and work function of the metal, Φ, to characterize the redox property of B-site metal. By comparing the interface conductivity of these samples with the thermodynamic phase diagram of B-site metals as shown in Fig. 5, we obtained the thermodynamic criterion for the formation of 2DEG at amorphous-ABO_3/KTO interface. Our results show that the smaller absolute value of ΔH_f^o and the larger value of Φ of the B-site metal would result in higher mobility of the two-dimensional electron gas that formed at the corresponding amorphous-ABO_3/$KTaO_3$ interface (under the premise of satisfying the thermodynamic criterion).

*Project supported by the National Key R&D Program of China (Grant Nos. 2016YFA0300701, 2017YFA0206304, and 2018YFA0305704), the National Natural Science Foundation of China (Grant Nos. 11934016, 111921004, 51972335, and 11674378), and the Key Program of the Chinese Academy of Sciences (Grant Nos. XDB33030200 and QYZDY-SSW-SLH020).

†Corresponding author. E-mail: yschen@iphy.ac.cn
‡Corresponding author. E-mail: jrsun@iphy.ac.cn

© 2021 Chinese Physical Society and IOP Publishing Ltd

2. Experimental methods

For the systematic study, various amorphous-ABO_3 oxides were selected to form the amorphous-ABO_3/$KTaO_3$ interfaces, including $CaZrO_3$ (CZO), $LaAlO_3$(LAO), $(LaAlO_3)_{0.3}(SrAl_{0.5}Ta_{0.5}O_3)_{0.7}$ (LSAT), $SrTiO_3$(STO), $KTaO_3$(KTO), $SrNbO_3$(SNO), $NdGaO_3$, $LaMnO_3$, $LaFeO_3$, $LaCoO_3$, and $LaCrO_3$. All the amorphous-ABO_3 layers were grown on the (001)-oriented KTO substrates ($3\times3\times0.5$ mm^3) by the technique of pulsed laser deposition (PLD). The laser fluence was 2 J/cm^2 and the pulse frequency was 2 Hz. During the growth process, the oxygen pressure was maintained at 2×10^{-3} Pa. The temperature of the substrate was fixed at 100 °C. After the growth process, all the samples were furnace cooled to room temperature without changing oxygen pressure.

The thickness of different amorphous-ABO_3 layer keeps at 5 nm, as evidenced by small angle x-ray reflectivity (XRR) measurements. The surface topography and flatness of these samples were observed by atomic force microscope (AFM). The transport behaviors were measured by a Quantum-Design physical property measurement system (PPMS) adopting the van der Pauw geometry.

3. Results and discussion

We take the amorphous-LAO/KTO sample as an example. Figure 1(a) shows the results of XRR measurements. The good agreement of the XRR oscillations between the testing result and simulation data indicates the high planeness of the as-deposited LAO layer. Curve fitting (black curve) reveals a layer thickness of 5 nm. Figure 1(b) is the surface topography of the film measured by AFM. The film is very smooth with a mean square root roughness of 0.2 nm in the area of 5×5 μm^2. These features were also confirmed in other samples, indicating the high quality of our amorphous-ABO_3/KTO samples.

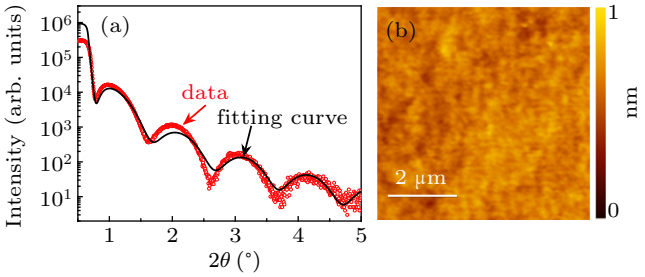


Fig. 1. (a) XRR curve of the amorphous-LAO film grown on KTO substrate. Black line is the fitting curve. (b) AFM image of the amorphous-LAO film deposited on KTO substrate.

Figure 2(a) is a schematic diagram of the device for measuring the electrical transport properties of amorphous-ABO_3/KTO heterostructure. Figure 2(b) shows the temperature dependence of the sheet resistance (R_s) for selected amorphous-ABO_3/KTO interfaces, which displays good metallic behavior: with the decrease of temperature, the sheet resistance decreases continuously. We characterize the metallicity by the ratio of sheet resistance measured at 300 K and 2 K. The higher R(300 K)/R(2 K) ratio means better metallicity. We find that R(300 K)/R(2 K) varies in a wide range, from the maximal ratio of ∼ 212 for the amorphous-KTO/KTO interface to the minimal ratio of ∼ 11 for the amorphous-LAO/KTO interface, i.e., the 2DEG formed at the KTO/KTO interface exhibits better metallicity. Notably, the metallic 2DEG appears only when the cap layer is LAO, CZO, STO, SNO, LSAT, or KTO. Obviously, the intrinsic properties of these cap layers will strongly affect the conduction characteristic at the interface. Hereafter, we will focus on these conducting interfaces.

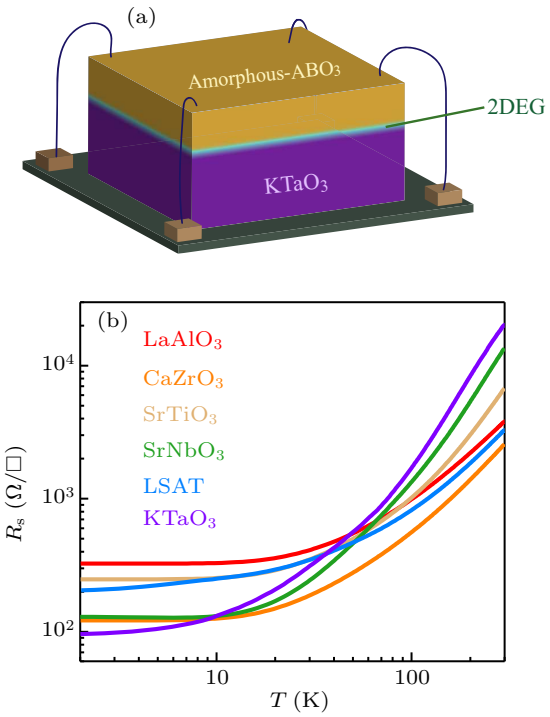


Fig. 2. (a) A sketch for the measurements of sheet resistance and Hall resistance. (b) Sheet resistance of amorphous-ABO_3/KTO interfaces as a function of temperature. The labels in the figure refer to the composition of the deposited amorphous-ABO_3 film.

To get further information about 2DEG, we performed the measurement of Hall resistance (R_{xy}) in the temperature interval from 2 K to 300 K. As an example, Fig. 3(a) shows the Hall resistance at 2 K, as a function of magnetic field (H). R_{xy} exhibits a linear variation with the applied field for all samples, i.e., only one species of charge carriers exists in the 2DEGs.[28] However, the R_{xy}–H slope (R_H) undergoes a considerable change with the cap layer, implying different carrier density (n_s) in different 2DEGs. In Fig. 3(b) we summarize the relationship between the carrier density and the cap layer, where n_s is determined by $n_s = -1/(e\cdot R_H)$. Corresponding to the maximal and minimal R(300 K)/R(2 K) ratios, amorphous-KTO/KTO exhibits the minimal carrier density of 2.9×10^{13} cm^{-2} and amorphous-LAO/KTO exhibits the maximal carrier density of 7.3×10^{13} cm^{-2}, respectively. Obviously, the capability to generate mobile electrons for different

cap layers varies ~ 2.5 times. Similar feature is observed in the R_{xy}–H curve obtained at other temperatures (not shown).

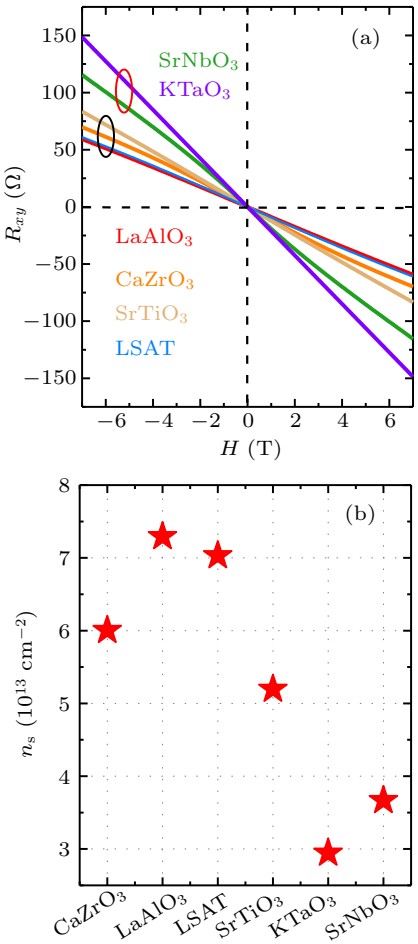


Fig. 3. (a) Hall effect of amorphous-ABO_3/KTO interfaces at 2 K (the labels in the figure refer to the composition of the deposited amorphous-ABO_3 film). (b) The sheet carrier density, n_s, versus the composition of the cap layer, obtained at 2 K.

To get a general idea about the temperature dependence of the carrier density, in Fig. 4 we show n_s and the corresponding mobility as functions of T, where the mobility is calculated based on the formula $\mu_s = 1/(e \cdot n_s \cdot R_s)$. The carrier density is the largest at 300 K and undergoes a decrease upon cooling. This feature is especially obvious in the interface with $CaZrO_3$ cap layer. It is an indication of charge localization. Correspondingly, the mobility experiences a rapid increase with the decrease of temperature. At low temperature, the dielectric constant of KTO grows, screening the electron scatter from ionic impurities. The maximal mobility at 2 K is 2209.41 $cm^2/V \cdot s$, occurring at the amorphous-KTO/KTO interface. From the amorphous-KTO/KTO to the amorphous-LAO/KTO interface, the mobility shows a rapid decrease.

The origin of the 2DEG is in hot debate since the discovery of the 2DEG in 2004. Three explanations are widely accepted, including polar discontinuity,[29] electron doping by oxygen vacancy,[30] and cation interdiffusion.[31] Compared with crystalline interface, the polar discontinuity at amorphous interface is strongly suppressed. Because of the low deposition temperature (100 °C), cation interdiffusion should be negligible. In contrast, previous experimental results have demonstrated that the outward oxygen diffusion plays a dominative role in the formation of 2DEG at the amorphous-LAO/STO interface.[32] We therefore ascribe the 2DEG at the amorphous-ABO_3/KTO interface to the redox reaction effect. Besides obtaining oxygen from the background atmosphere, in fact, the cap layer will also extract oxygen from the interfacial layer of the $KTaO_3$ substrate. When the content of oxygen vacancies is high enough, 2DEG forms.

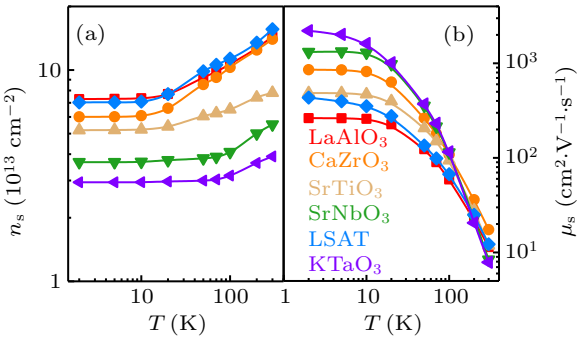


Fig. 4. (a), (b) Carrier density, n_s, and Hall mobility, μ_s, versus temperature, respectively, for all the KTO-based heterostructures. The corresponding cap layers are denoted in (b). The solid lines are guides to the eyes.

Fu *et al.*[33] have performed a research on the redox reaction when a metal film is deposited on the surface of $SrTiO_3$ at room temperature. They put forward a thermodynamic criterion for redox reaction. According to this work, redox reaction has a close relation to the formation heat of metal oxide, ΔH_f^o, and the work function of the metal, Φ. The former describes the ability to get oxidized for an element and the latter characterizes the electronegativity. Obviously, a high ΔH_f^o implies a strong tendency towards oxidization for an element. For the B-site metal in amorphous films, formation heat of metal oxide ΔH_f^o and work function Φ can be obtained from former literature[34] that are summarized in Fig. 5. The B-site metals marked by red circles represent for the insulated ABO_3/KTO interfaces, whereas the B-site metals marked by green symbols correspond to the interfaces with metallic conductivity. The orange-colored diamond represents for a special case, the semiconductive amorphous-$NdGaO_3$/$KTaO_3$ interface. Moreover, for the metallic ABO_3/KTO interfaces, a small ΔH_f^o for the B-site metals usually gives higher mobility, which are marked as green stars. Correspondingly, the B-site metals with large ΔH_f^o and lower mobility are marked as green squares. Based on this analysis, we obtain a thermodynamic criterion for the redox reactions at the KTO interface, which is labeled as the shaded area. The formation heat of metal oxide, ΔH_f^o, should be lower than -350 kJ/(mol O) and the work function of the metal, Φ, should locate in the range of $3.75\ \text{eV} < \Phi < 4.4\ \text{eV}$.

Remarkably, Nb and Ta, corresponding B-site metals of $SrNbO_3$ and $KTaO_3$, locate on the border region for the occurrence/nonoccurrence of redox reaction. This explains the low

carrier density at the interface of the amorphous-KTO/KTO and the amorphous-SNO/KTO samples. On the other hand, the carrier density at their interface is low but the carrier mobility is high. Among them, the carrier mobility of the amorphous-KTO/KTO interface can reach 2209.41 $cm^2/V{\cdot}s$ at 2 K. This provides a guide to prepare $KTaO_3$-based 2DEGs of high mobility at a deposition temperature of 100 °C, that is, for the B-site metal in deposited amorphous-ABO_3 film, the absolute value of the formation heat of metal oxide is as small as possible and the value of the work function of the metal is as large as possible (under the premise of satisfying the thermodynamic criterion mentioned above).

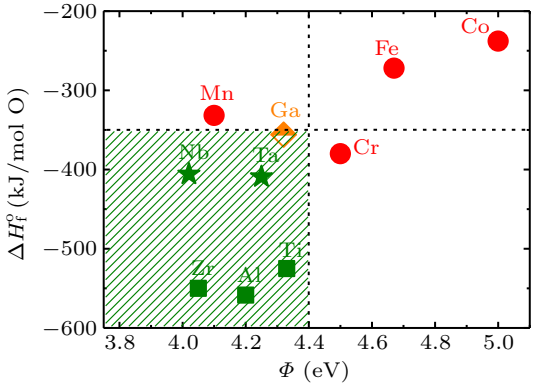


Fig. 5. Formation heat of metal oxides versus the work function of B-site metals for the ABO_3/KTO interfaces. For metallic interfaces, the B-site metals locate mainly in the region of $\Delta H_f^\circ < -350$ kJ/(mol O) and 3.75 eV $< \Phi <$ 4.4 eV (shaded area).

4. Conclusion

In summary, we systematically investigated the effect of the redox properties of the B-site metal on 2DEGs transport characteristics at amorphous-ABO_3/$KTaO_3$ interfaces, by varying the composition of the cap layer. We found that metallic conductive interface can be created when the amorphous film has Zr, Al, Ti, Ta, or Nb elements at the B sites. Whereas the interface is insulating when the overlayer has Mn, Fe, Co, or Cr elements at the B sites. By summarizing the interface conductivity of these samples, we obtained the thermodynamic criterion for the redox reaction at the transition metal oxide/KTO interface. Finally, we provided a guideline on searching for $KTaO_3$-based 2DEGs of high mobility. This work has certain guiding significance for finding high performance two-dimensional electron gas, and takes a solid step for the application of oxide electronic devices.

References

[1] Ohtomo A and Hwang H Y 2004 *Nature* **427** 423
[2] Hotta Y, Susaki T and Hwang H Y 2007 *Phys. Rev. Lett.* **99** 236805
[3] Kim J S, Seo S Sea A, Chisholm M F, Kremer R K, Habermeier H U, Keimer B and Lee H N 2010 *Phys. Rev. B.* **82** 201407
[4] Biscaras J, Bergeal N, Kushwaha A, Wolf T, Rastogi A, Budhani R C and Lesueur J 2010 *Nat. Commun.* **1** 89
[5] Chen Y Z, Pryds N, Kleibeuker J E, Sun J R, Stamate E, Koster G, Shen B G, Rijnders G and Linderoth S 2011 *Nano. Lett.* **11** 3774
[6] Li C, Xu Q F, Wen Z F, Zhang S T, Li A D and Wu D 2013 *Appl. Phys. Lett.* **103** 201602
[7] Gunkel F, Skaja K, Shkabko A, Dittmann R, Hoffmann-Eifert S and Waser R 2013 *Appl. Phys. Lett.* **102** 071601
[8] Chen Y Z, Bovet N, Trier F, Christensen D V, Qu F M, Andersen N H, Kasama T, Zhang W, Giraud R, Dufouleur J, Jespersen T S, Sun J R, Smith A, Nygard J, Lu L, Büchner B, Shen B G, Linderothand S and Pryds N 2013 *Nat. Commun.* **4** 1371
[9] Huang Z, Han K, Zeng S W, Motapothula M, Borisevich A Y, Ghosh S, Lü W M, Li C J, Zhou W X, Liu Z Q, Coey M, Venkatesan T and Ariando 2015 *Nano Lett.* **16** 2307
[10] Chen Y Z, Trier F, Kasama T, Christensen D V, Bovet N, Balogh Z I, Li H, Thydén K T S, Zhang W, Yazdi S, Norby P, Pryds N and Linderoth S 2015 *Nano Lett.* **15** 1849
[11] Wang F N, Li J C, Zhang X M, Liu H Z, Liu J, Wang C L, Zhao M L, Su W B and Mei L M 2017 *Chin. Phys. B.* **26** 037101
[12] Qi S J, Sun X, Yan X, Zhang H, Zhang H R, Zhang J E, Huang H L, Han F R, Song J H, Shen B G and Chen Y S 2021 *Chin. Phys. B.* **30** 017301
[13] Reyren N, Thiel S, Caviglia A D, Kourkoutis L F, Hammerl G, Richter C, Schneider C W, Kopp T, Rüetschi A S, Jaccard D, Gabay M, Muller D A, Triscone J M and Mannhart J 2007 *Science* **317** 1196
[14] Caviglia A D, Gariglio S, Reyren N, Jaccard D, Schneider T, Gabay M, Thiel S, Hammerl G, Mannhart J and Triscone J M 2008 *Nature* **456** 624
[15] Brinkman A, Huijben M, van Zalk M, Huijben J, Zeitler U, Maan J C, van der Wiel W G, Rijnders G, Blank and Hilgenkamp H 2007 *Nat. Mater.* **6** 493
[16] Kalisky B, Bert J A, Klopfer B B, Bell C, Sato H K, Hosoda M, Hikita Y, Hwang H Y and Moler K A 2012 *Nat. Commun.* **3** 922
[17] Lee J S, Xie Y W, Sato H K, Bell C, Hikita Y, Hwang H Y and Kao C C 2013 *Nat. Mater.* **12** 703
[18] Trier F, Prawiroatmodjo G, Zhong Z, Christensen D, Soosten M, Bhowmik A, Lastra J, Chen Y, Jespersen T and Pryds N 2016 *Phys. Rev. Lett.* **117** 096804
[19] Lesne E, Fu Y, Oyarzun S, Rojas-Sánchez J C, Vaz D C, Naganuma H, Sicoli G, Attané J P, Jamet M, Jacquet E, George J M, Barthélémy A, Jarès H, Fert A, Bibes M and Vila L 2016 *Nat. Mater.* **15** 1261
[20] Song Q, Zhang H R, Su T, Yuan W, Chen Y Y, Xing W Y, Shi J, Sun J R and Han W 2017 *Sci. Adv.* **3** e1602312
[21] Zou K, Ismail-Beigi S, Kisslinger K, Shen X, Su D, Walker F J and Ahn C H 2015 *APL Mater.* **3** 036104
[22] Harashima S, Bell C, Kim M, Yajima T, Hikita Y and Hwang H Y 2013 *Phys. Rev. B.* **88** 085102
[23] Höchli U T, Weibel H E and Boatner L A 1977 *Phys. Rev. Lett.* **39** 1158
[24] King P D C, He R H, Eknapakul T, Buaphet P, Mo S K, Kaneko Y, Harashima S, Hikita Y, Bahramy M S, Bell C, Hussain Z, Tokura Y, Shen Z X, Hwang H Y, Baumberger F and Meevasana W 2012 *Phys. Rev. Lett.* **108** 117602
[25] Zhang H, Zhang H R, Yan X, Zhang X J, Zhang Q H, Zhang J, Han F R, Gu L, Liu B G, Chen Y S, Shen B G and Sun J R 2017 *ACS Appl. Mater. Interfaces* **9** 36456
[26] Zhang H, Yan X, Zhang X J, Wang S, Xiong C M, Zhang H R, Qi S J, Zhang J E, Han F R, Wu N, Liu B G, Chen Y S, Shen B G and Sun J R 2019 *ACS Nano* **13** 609
[27] Zhang H R, Yun Y, Zhang X J, Zhang H, Ma Y, Yan X, Wang F, Li G, Li R, Khan T, Chen Y S, Liu W, Hu F X, Liu B G, Shen B G, Han W and Sun J R 2018 *Phys. Rev. Lett.* **121** 116803
[28] Joshua A, Pecker S, Ruhman J, Altman E and Ilani S 2012 *Nat. Commun.* **3** 1129
[29] Nakagawa N, Hwang H Y and Muller D A 2012 *Nat. Mater.* **5** 204
[30] Basletic M, Maurice J L, Carrétéro C, Herranz G, Copie O, Bibes M, Jacquet É, Bouzehouane K, Fusil S and Barthélémy A 2008 *Nat. Mater.* **7** 621
[31] Willmott P R, Pauli S A, Herger R, Schlepütz C M, Martoccia D, Patterson B D, Delley B, Clarke R, Kumah D, Cionca C and Yacoby Y 2007 *Phys. Rev. Lett.* **99** 155502
[32] Herranz G, Basletic M, Bibes M, Carrétéro C, Tafra E, Jacquet E, Bouzehouane K, Deranlot C, Hamzic A, Broto J M, Barthélémy A and Fert A 2007 *Phys. Rev. Lett.* **98** 216803
[33] Fu Q and Wagner T 2007 *Surf. Sci. Rep.* **62** 431
[34] Lide D R 2010 *CRC Handbook of Chemistry and Physics* [M], 92nd (Boca Raton: CRC Press) pp. 5–5, 5–10, 5–12, 5–15, 5–16, 5–17, 12–114